AIAA JOURNAL
Vol. 44, No. 3, March 2006

# Linear Stochastic Estimation of a Swirling Jet

Ephraim J. Gutmark* and Swann Verfaillie†
*University of Cincinnati, Cincinnati, Ohio 45221-0070*
Jean-Paul Bonnet‡
*University of Poitiers, F-86034 Poitiers, France*
and
Fernando Grinstein§
*U.S. Naval Research Laboratory, Washington, D.C. 20375-5344*

**Linear stochastic estimation (LSE) was applied to study the coherent structures of a highly swirling jet. The swirling jet was produced by a triple annular swirler (TAS) featuring three concentric swirling flows that merge into a turbulent swirling jet. The LSE used statistical theory to provide an estimate of the instantaneous flowfield by reproducing, in space and time, the large-scale coherent structures of the flow using minimum experimental information. LSE turned out to be very efficient for extracting coherent structures from the turbulent flowfield and for describing their dynamics. Although the LSE is highly dependent on the levels of correlation, it enabled the reconstruction of the complete coherent flowfields from the knowledge of only few near-field acoustic signals, providing an effective tool for data reduction to formulate turbulent inflow boundary conditions for large-eddy simulation.**

## I. Introduction

PREVALENT approaches in experimental and computational fluid mechanics focus on the characteristics and dynamics of coherent structures (CS) that exist in turbulent flows. The existence of such coherent motions and the crucial role they play in practical processes such as mixing, noise, vibrations, heat transfer, and drag has been well known for nearly three decades. CS are sources of high Reynolds stresses and high turbulent kinetic energy, and therefore they play a crucial role in mixing, development, and stability of the flow.[1–4] Coherent structures are usually defined as flow structures whose size is comparable to the spanwise dimension of the flow and whose evolution highly depends on the initial conditions.

Because CS are typically embedded in a chaotic and random field, the challenge for both experimentalists and computational-fluid-dynamics investigators is to separate them from the turbulent background. Several eduction methods have been widely studied and most of their characteristics are understood. Periodic or quasi-periodic events are easily detected by spatial correlation functions and spectral techniques. Numerous other methods for coherent structure extraction include conditional sampling, pattern recognition, four-quadrants analysis, wavelets theory, and the variable-integration time average. The use of linear stochastic estimation (LSE)[1,5–7] to generate inflow boundary conditions (BCs) for direct numerical simulation (DNS) was demonstrated by Druault.[8] He studied the impact of inflow specifications on the DNS of a plane turbulent mixing layer. Bonnet et al.[9] and Lewalle et al.[10] estimated a mixing-layer field using LSE. The estimated velocity components through the mixing layer have been computed from the actual velocity components extracted at selected positions across the mixing layer. Picard and Delville[11] estimated the velocity field of a jet mixing layer using LSE with pressure signals as the reference. The centers of the coherent structures that were extracted by this technique corresponded to the low levels of the pressure signals.

The sensitivity of turbulent flows to inflow BCs is now well recognized[12]: the far-field portions of turbulent flows remember their particular near-field features. The transition from initial (inflow) conditions to the associated asymptotic flow involves unsteady large-scale coherent-structure dynamics, which can be captured by LES but not by single-point closure turbulence modeling (i.e., Reynolds-averaged Navier–Stokes approaches). Considering the typical availability of single-point statistical data, there is no unique way to reconstruct a three-dimensional unsteady velocity field with turbulent eddies that can be used as realistic inflow BCs; such data have been shown to be typically insufficient to parameterize turbulent inflow BCs for LES of inhomogeneous flows.[13]

Two critical LES issues include the treatment of the unresolved (subgrid-scale) flow features and the required BC modeling. Although subgrid-scale modeling issues have motivated intense research in the last 30 years, less attention has been typically devoted to the equally relevant BC aspects, and their importance is often overlooked. Because actual BC choices select flow solutions,[14] emulating particular flow realizations demands precise characterization of their inflow and other relevant conditions at open outflow or at solid and other facility boundaries. This flow characterization issue is a challenging one when laboratory or field realizations are involved because the available information is typically insufficient. Achieving closure of the BC model based on laboratory data requires identifying appropriate data acquisition and its suitable postprocessing (i.e., reduction) for effective use in the simulations. Because the flow is thus more or less driven by the inflow conditions, prescribed realistic turbulent fluctuations must be able to achieve some sort of equilibrium with imposed mean flow and other boundary conditions. The inherent inability to carry out this inflow BC reconstruction properly in the simulations leads to needing a transition inflow region, over which the imposed flow conditions can evolve into realistic turbulent velocity fluctuations, after allowing for feedback effects to occur as the simulation progresses. Such approaches[15] include using precursor simulations to separately generate/store unsteady planes of inflow data, extraction/rescaling techniques,[16] and forced synthetic inflow turbulence generation,[17] all of which have been extensively tested for channel flow problems. The challenge is how to minimize the length of this developmental region because its presence adds to overall computational cost, through additional number of grid points involved and actual extra required data processing near the inflow.

Received 30 July 2005; accepted for publication 24 September 2005. 

*Professor and Ohio Regents Eminent Scholar, Department of Aerospace Engineering and Engineering Mechanics.
†Graduate M.S. Student, Department of Aerospace Engineering and Engineering Mechanics.
‡Professor, Laboratories for Aerodynamic Studies.
§Research Physicist, Laboratory for Computational Physics and Fluid Dynamics; currently Staff Member, Applied Physics Division, Los Alamos National Laboratory, Los Alamos, NM 87545.

Because of performance requirements on the design of gas turbine engines, there is considerable interest in identifying optimal swirl and geometrical conditions to achieve specific practical goals in actual flight regimes, such as reduced emissions, improved efficiency, and stability. In the context of research swirl flow combustor simulations designed to address these goals, hybrid simulation approaches have been proposed[18] in which effective inlet boundary conditions are prescribed at the outlet of a fuel-injector nozzle based on Reynolds-averaged Navier–Stokes (RANS) or laboratory data, and large-eddy simulation (LES) is used to study the unsteady swirl flow dynamics downstream. Such approaches are intended to avoid dealing with the significant computational cost of simulating the flow within the complex multiswirler fuel mixer. More generally, however, such hybrid approaches and effective BCs are also needed in practical simulations of very large (full-scale) systems, where separate (RANS or LES) flow solvers are used in each component, and large-scale unsteady flow information between solvers must be exchanged at the interfaces between domains.[19]

In this context, it is not practical to arbitrarily vary an inlet length to implement a turbulent inflow BC because that length can typically control desirable coupling between modes characterizing the flow in the connecting domains. Specifically, combining swirling flow motion with sudden expansion to the full combustor diameter provides an effective way of enhancing the fuel-air mixing and stabilizing combustion, with the actual coupling between swirl and sudden expansion instabilities depending on the relative length of the inlet.[18] An additional challenging difficulty relates to emulating the typically high turbulent intensities at a swirler outlet largely associated with CS (swirl) contributions to the inlet velocity fluctuations. For example, relatively large peak fluctuation levels (as high as 50% of peak mean velocities) are typical at the outlet plane of a triple annular swirler (TAS) multiswirler such as considered in the present work.[18]

Prescribing realistic turbulent inflow BCs thus leads to requiring fairly nontrivial laboratory data acquisition (e.g., space/time correlated) and developing its adequate postprocessing (reduction). The prescribed inflow velocity boundary condition normally consists of mean profiles and superimposed fluctuations. Prescribing an inflow quantity $u$ (a velocity component) at each point of an inflow plane is typically required. At each grid point of the inflow plane, we can split $u$ into its mean and fluctuating parts, $u = U + u'(t)$. The challenge is how to prescribe realistic velocity fluctuations $u'(t)$ using the available laboratory information in such a way that the prescription can be in some reasonable consistent equilibrium with the mean flow.

In the present paper, LSE is discussed as a tool for description of flow dynamics and for structure identification in the context of a swirling jet. The LSE uses statistical theory to provide an estimate of the instantaneous flowfield by reproducing, in space and time, the large-scale coherent structures of the flow using minimum experimental information, to estimate the flowfield based on its near-field acoustics.

## II. Experimental Setup

The TAS is characterized by three concentric swirling flows that merge into a turbulent three-dimensional swirling flow[20] (Fig. 1). The external flow is provided by eight radial slots, whereas the intermediate and internal flows pass through four axial vanes. The configuration used in the present tests was: 55 deg clockwise for the external flow, 45 deg clockwise for the intermediate flow, 45 deg clockwise for the internal flow.

### A. Setup for Correlation Studies Using Hot-Wire Measurements

To characterize the swirling flow in terms of correlations, two series of tests using hot-wire anemometry and pressure measurements were conducted: one in the streamwise plane and the other in a cross section of the jet. The apparatus used in both experiments remained the same:

1) For the cold-flow test rig, room-temperature air passes through the TAS nozzle after being conditioned in a chamber equipped with screens and honeycomb. A valve and a flow-meter allow the selection the desired mass flow rate.

2) Three-dimensional traverse enables mapping of the desired flowfield on any predetermined grid and is computer controlled.

3) With TSI single hot wire and its anemometer IFA200, a single hot wire has been used. The calibration has been conducted in a special calibration rig.

4) Pressure was measured using Bruel and Kjaer $\frac{1}{4}$-in. (6.35-mm) microphones and amplifiers.

5) The acquisition was performed using a National Instruments acquisition card type PCI-6052E and its eight analog inputs connecting board type BNC-2110.

The first experiment, whose setup is shown in Fig. 2, investigated the correlations between the near-field pressure (13 mm from the edge of the jet) and the velocity field in the jet centerline plane. The traversing grid for the hot wire was determined based on previous studies on the TAS swirling jet that showed an approximate spreading angle of 30 deg. (The microphone stayed in a fixed location.) The jet was traversed at four different axial distances from the nozzle exit (0.25, 0.75, 1.25, and 1.75 in., or 6.35, 19.05, 31.75, and 44.45 mm) at a radial step size of 0.2 in. (5.1 mm) and an increasing number of data points to cover the increased width of the jet. Because of the high temporal resolution of the hot wire and the microphone, a sampling rate of 10 kHz was chosen, and 32,000 samples were taken at each location. The acquisition card had a sampling rate of 300 kS/s such that the time delay between the velocity and the pressure channels was 3.33 $\mu$s and was negligible compared to the time accuracy of the sensors.

The test conditions are given here:

1) Atmospheric conditions are 29.07 In Hg ($\approx$0.97 atm) and 77°F ($\approx$25°C).

2) Flow conditions are $Qm = 67$ standard cubic feet per minute (SCFM) ($\approx$1.9 m$^3$/min) $\rightarrow U_{\text{axial}} = (4 \times Q_m)/(\pi \times D) \approx 15.6$ m/s.

3) Pressure drop is $\Delta P = 6.2$ psi ($\approx$42,750 Pa).

4) Reynolds number is $5.2 \times 10^4$.

5) Swirl number is 0.4.

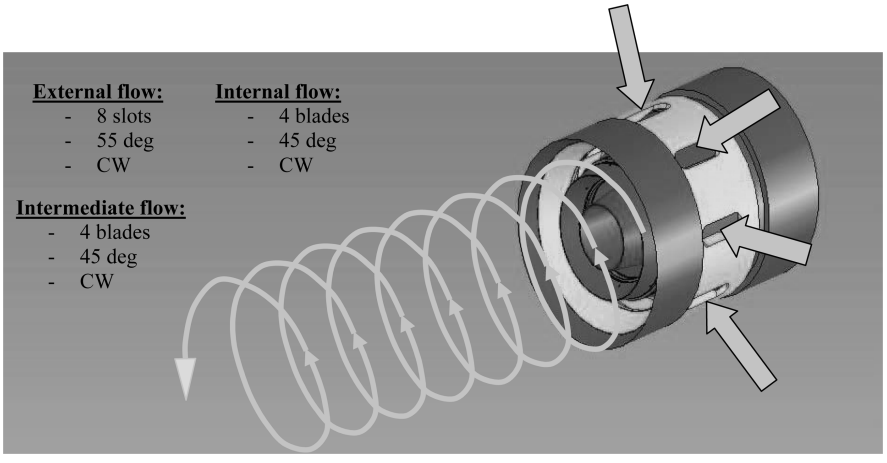


**Fig. 1 Triple annular swirler (TAS).**

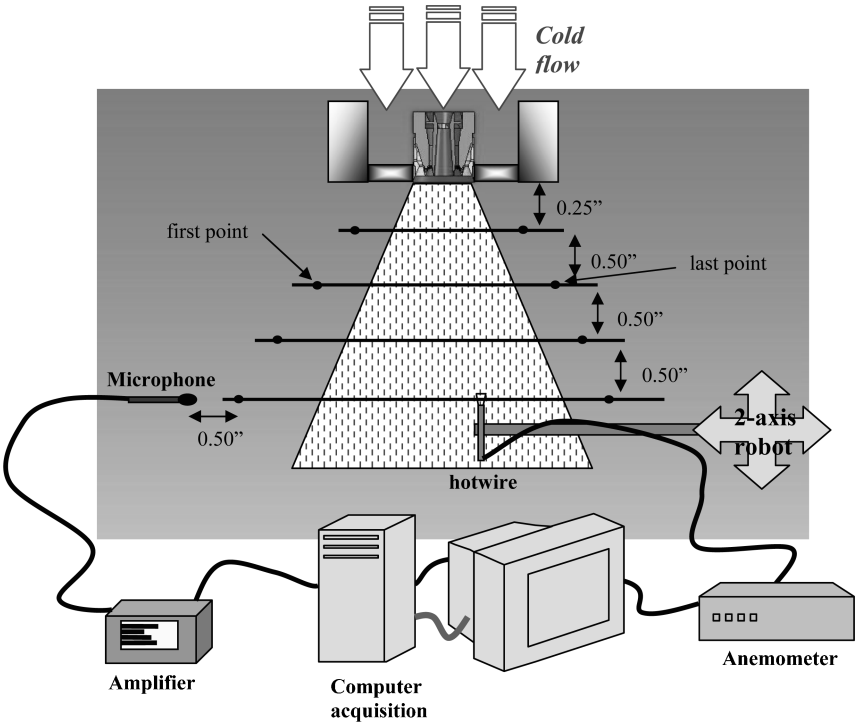


**Fig. 2 Schematic of the hot-wire scanning area on the center axial plane.**

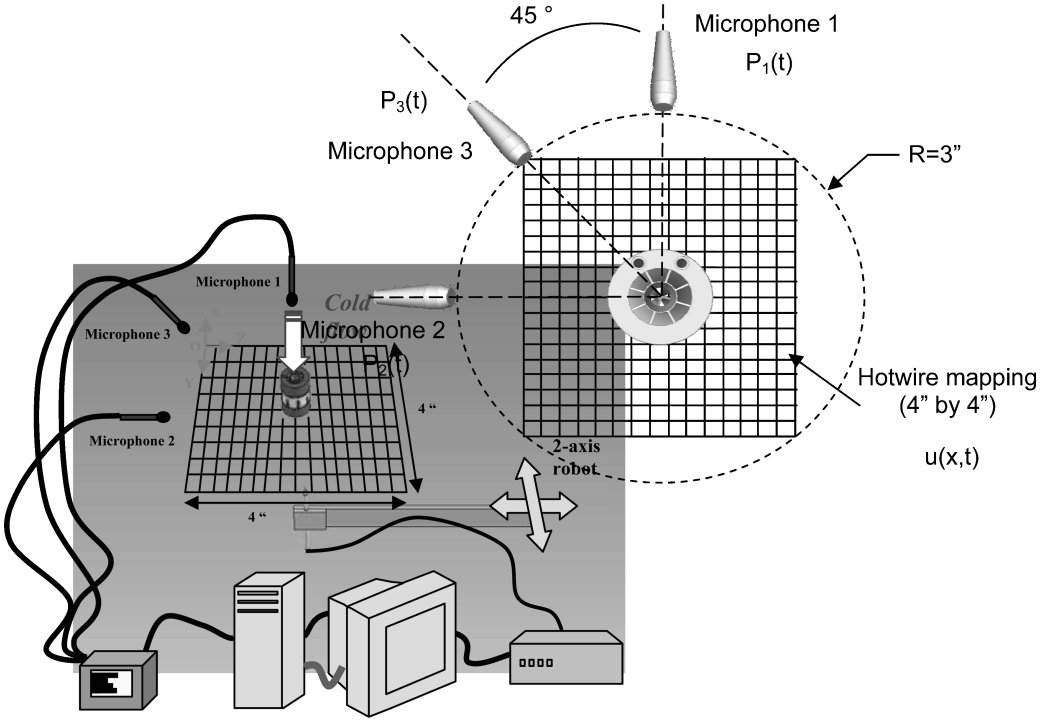


**Fig. 3 Schematic of the hot-wire LSE experimental setup.**

### B. Setup for LSE Analysis Using Traversing Hot Wire and Microphones

The experimental setup for the LSE in Fig. 3 is the same as the one used for measuring the correlations except that three microphones were used. The microphones were located on a 76-mm circle centered on the TAS and were equally spaced by 45 deg. This arrangement enabled the hot-wire scan over the 102 × 102 mm velocity grid without mutual interference. The acquisition plane was at 6.35 mm from the nozzle with the same test conditions as just given.

### C. Streamwise Configuration of the Particle-Image-Velocimetry Studies

The setup is shown in Fig. 4. Two cameras were located 30 in. from the jet and covered an area of 120 × 160 mm (4.7 × 6.3 in.) on the jet center plane. Eight microphones were aligned along the jet edge, close enough to acquire better correlations yet avoiding any interference with the jet flow. A 30-deg spreading angle of the jet was assumed based on previous hot-wire measurements. The particle-image-velocimetry (PIV) system recorded data at a frequency of

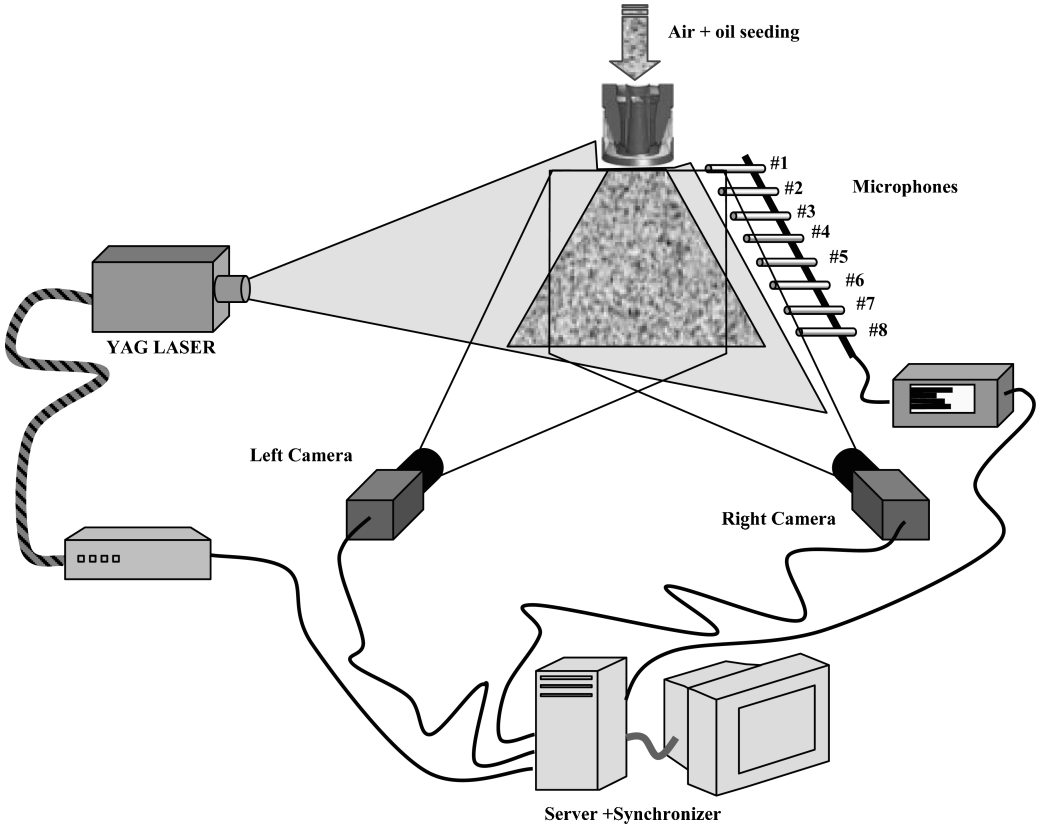


**Fig. 4 Schematic of the PIV streamwise experimental setup.**

1 Hz, a rate that allowed the recording of pressure on an extended time window, and at a sampling rate of 40 kHz it was possible to digitize 400 pressure data points. This synchronization made it possible to adjust accurately the pressure measurements with the velocity data. To improve the accuracy of this synchronization, the highest correlations between the pressure measurements of each microphone and the velocity field were selected.

### D. Cross-Sectional Configuration of the PIV Studies

The schematic of the setup is shown in Fig. 5. The two PIV charge-coupled-device cameras were set at an angle of 30 deg relative to the centerline. The microphones arrangement consisted of eight microphones equally spaced circumferentially around the jet. They were located near the jet (about 13 mm), to obtain good correlations, in a plane which was 0.5 in. (12.7 mm) downstream from the nozzle exit. To avoid reflections of the laser beam from the microphone array, the velocity measurement plane was separated from the microphone plane by 1.25 in. (32 mm). This spatial offset resulted in a time delay that was taken into consideration when setting the signal synchronization. The synchronization was performed using several pressure samples for each snapshot, but the pressure measurements were initiated earlier in order to ensure that one of the 400 pressure points will overlap the PIV image.

## III. Results and Discussion

### A. Hot-Wire Correlation Studies

The mean velocity profiles at the four different distances are shown in Fig. 6. The high velocities at the outer edges of the jet are caused by the external and intermediate swirling flows that merge into a strong outer flow. The middle hump is caused by the flow of the internal swirler.

To study the relationship between the pressure and the velocity field, the relevant measures were the coherence function and the correlation coefficient.

1) The coherent function between the pressure $p$ and the velocity $v$ was defined by the power spectra of $p$ and $v$ and the cross spectrum between them:

$$C_{\mathrm{pv}}(f) = \frac{|P_{\mathrm{pv}}(f)|^2}{P_{\mathrm{pp}}(f)P_{\mathrm{vv}}(f)}$$

The coherence between the pressure and the velocity is decreasing as the distance between the microphone and the hot wire is increasing and the coherence is also decreasing at the downstream locations. The coherence is always maximum at a frequency of 110 Hz, which was characteristic to the flow at the present test conditions.

2) The correlation coefficient is a normalized measure of the strength of the linear relationship between the pressure and velocity. The correlation coefficient is related to the covariance by

$$R_{\mathrm{pv}} = \frac{Cov(p, v)}{\sqrt{Cov(p, p)Cov(v, v)}}$$

The correlation coefficient quantifies the level at which two variables are linearly dependent. This parameter is thus relevant for the study regarding the relations between the pressure and the velocity as a function of the location in the jet. The results for the four heights are shown in Fig. 7.

The correlation decreases with the distance between the two probes, from 0.47 (in the best case-axial distance of 0.25 in. or 6.35 mm) when the microphone and the hot wire are very close (13–20 mm) down to near-zero values when the hot wire is located at the opposite side of the jet. In the same way, the correlation is decreasing as the hot wire and microphone move downstream, but not because of the distance between the two probes, for the microphone remains aligned with the hot wire, but rather because the flow is losing its coherence in the downstream direction.

A close look at the evolution of the correlation while crossing the jet reveals that the coefficient is alternating between maximum

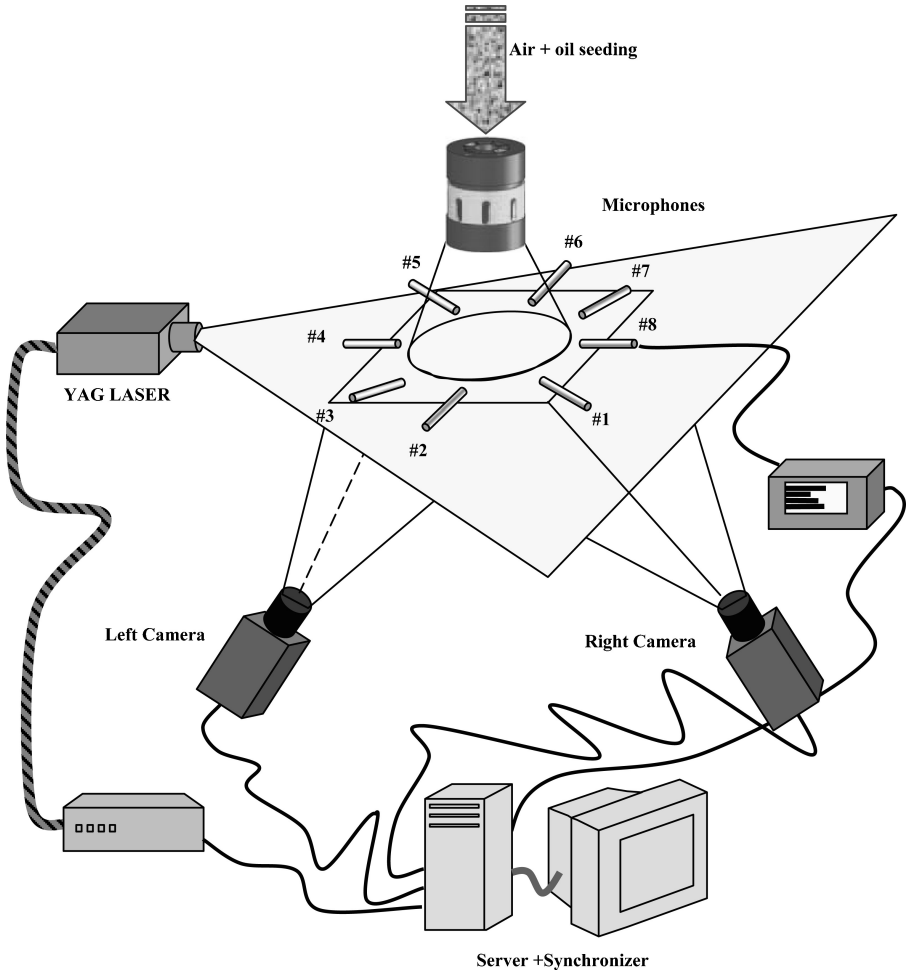


**Fig. 5 Schematic of the experimental setup for cross-sectional PIV measurements.**

and minimum values. The correlation between the pressure and the velocity across the jet is successively positive and negative: this behavior, which appears in a similar way at different axial distances, is related to the strong swirling characteristics of the jet. The distance between two succesive high correlation peaks is increasing in the downstream direction.

The relative high level of the cross correlations between pressure-velocity and pressure-pressure (not shown here) make this flow amenable to the application of LSE.

### B. LSE Analysis Using Hot Wire and Microphones

Prior to computing the LSE of the flowfield, the velocity profile and the correlation maps were obtained for the three microphones (Fig. 8). The correlation coefficients are about 0.2 as a result of the relatively large distance of the microphones from the flowfield (19 mm from the jet center). Additional circumferential microphones can improve the average correlation levels. However the correlations are still high enough to enable application of the LSE analysis, especially in the regions that are closer to the microphones. Even at this relatively low correlation level, it is possible to identify the spiral structure of the flow all of the way to the flow center.

The LSE analysis was performed by computing the correlation for each location at different times and not simultaneously. The estimation of the velocity $\tilde{u}(x,t)$ is given by a linear combination of the three pressure signals $p_1(t)$, $p_2(t)$, and $p_3(t)$ according to

$$\tilde{u}(x,t) = a_1(x)p_1(t) + a_2(x)p_2(t) + a_3(x)p_3(t)$$

where $a_i(x)$ are the stochastic coefficients that depend only on location. They provide the relationship between the fluctuating velocity at a certain location in the flowfield to the corresponding pressure that was measured adjacent to the flowfield. They are measured and computed by solving the following set of equations at each location:

$$\langle u(x,t)p_1(t)\rangle = a_1(x)\langle p_1(t)p_1(t)\rangle + a_2(x)\langle p_2(t)p_1(t)\rangle + a_3(x)\langle p_3(t)p_1(t)\rangle$$

$$\langle u(x,t)p_2(t)\rangle = a_1(x)\langle p_1(t)p_2(t)\rangle + a_2(x)\langle p_2(t)p_2(t)\rangle + a_3(x)\langle p_3(t)p_2(t)\rangle$$

$$\langle u(x,t)p_3(t)\rangle = a_1(x)\langle p_1(t)p_3(t)\rangle + a_2(x)\langle p_2(t)p_3(t)\rangle + a_3(x)\langle p_3(t)p_3(t)\rangle$$

$$a_i(x) = \begin{bmatrix} a_{i,11} & \cdot & \cdot & \cdot & a_{i,1n} \\ \cdot & \cdot & \cdot & \cdot & \cdot \\ \cdot & \cdot & \cdot & \cdot & \cdot \\ \cdot & \cdot & \cdot & \cdot & \cdot \\ a_{i,n1} & \cdot & \cdot & \cdot & a_{i,nn} \end{bmatrix}_{n\times n}$$

In the present case, in which the flowfield is given in a $32 \times 32$ grid, the estimate of the velocity is reduced to three $32 \times 32$ constant matrices $a_1(x)$, $a_2(x)$, and $a_3(x)$ and the time evolution of three near-field pressure measurements $p_1(t)$, $p_2(t)$, and $p_3(t)$. The correlations were made over 12,000 samples for each location of the 1024 grid points, and consequently the computation time was rather large (up to 10 min) because a large number of samples was required to reach the statistical convergence needed for the LSE analysis.

Figure 9 shows the result of the estimated velocity field at different successive times ($t = 0$, 0.5, 0.75, and 1 ms). The estimation of the fluctuating velocity enables the following of the evolution of the structure during the four different time steps. The swirling motion of the structures follows the swirling correlation structures that were

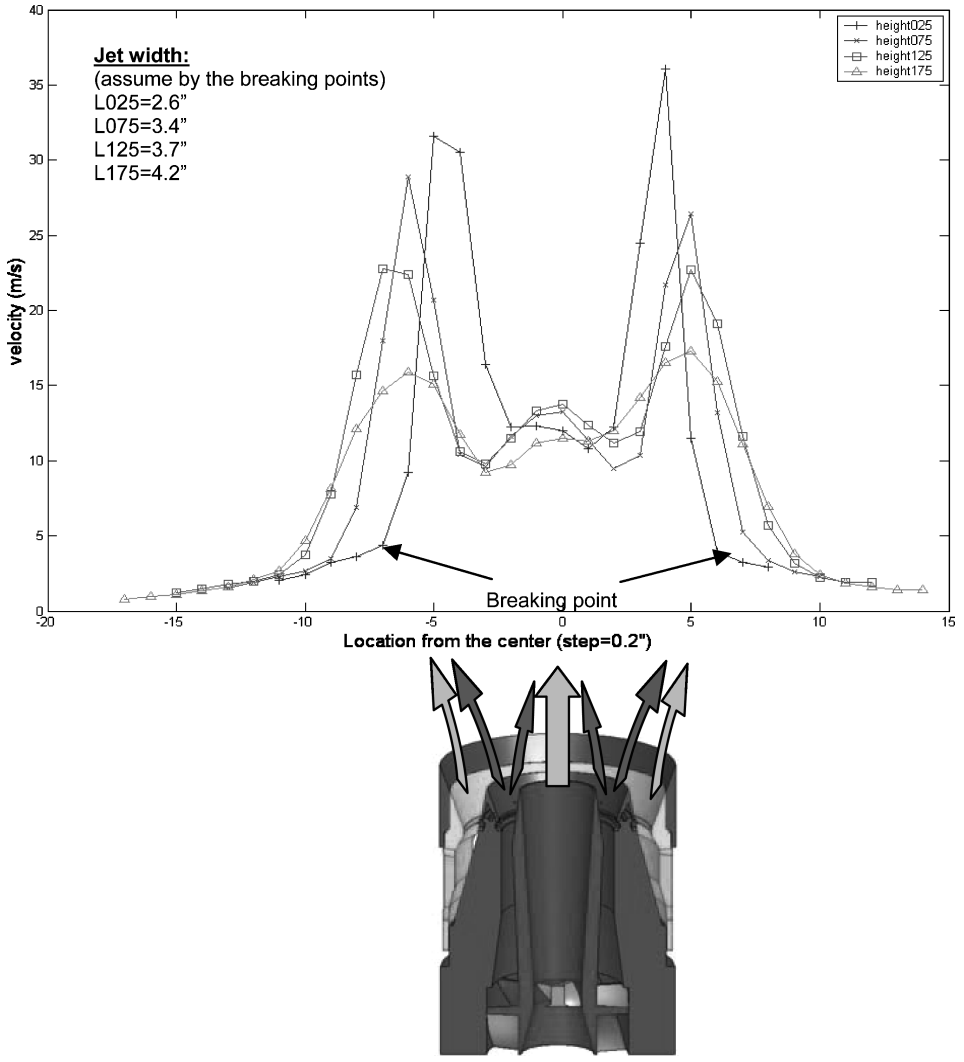


**Fig. 6 Velocity profiles at different axial locations.**

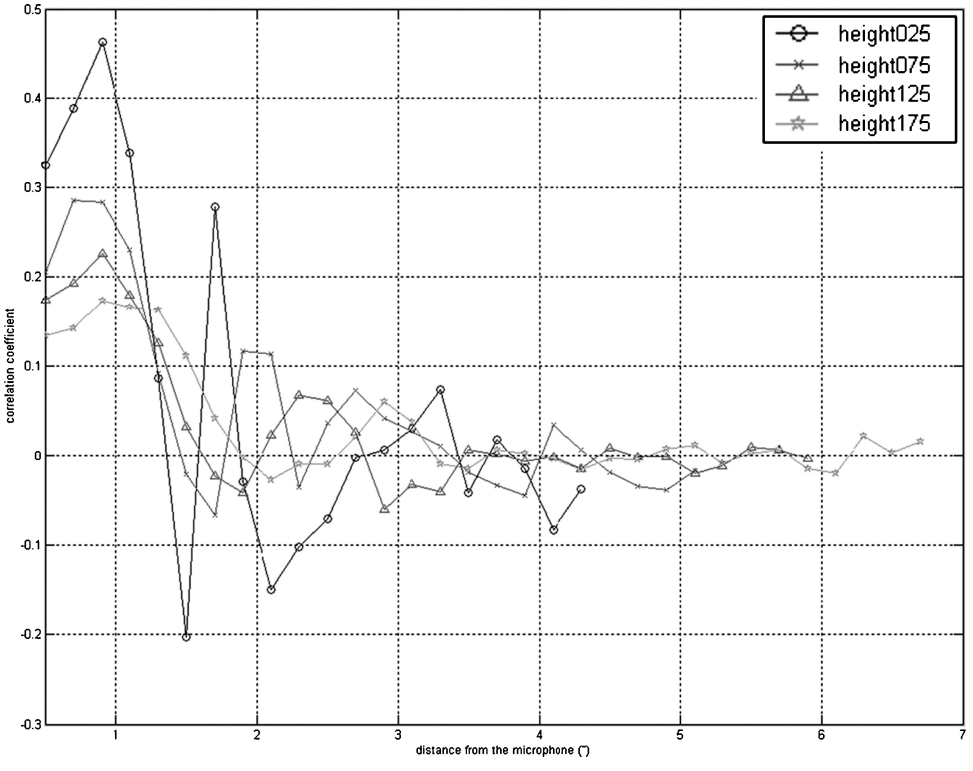


**Fig. 7 Evolution of the correlation coefficient with the distance from the microphone for different axial distances.**

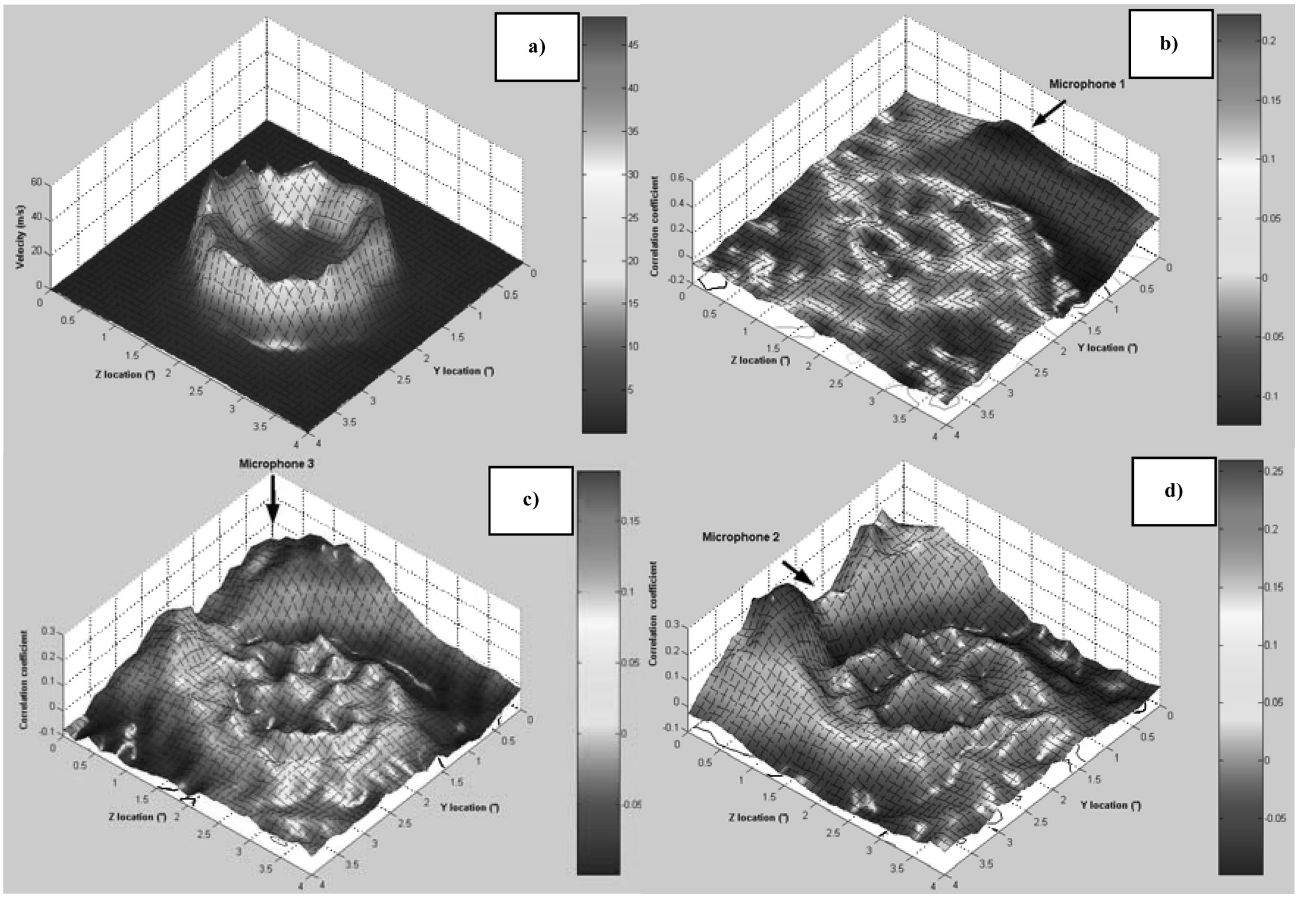


**Fig. 8 Velocity and correlative profiles for the different microphones: a) velocity profile, b) microphone 1 correlation, c) microphone 3 correlation, and d) microphone 2 correlation.**

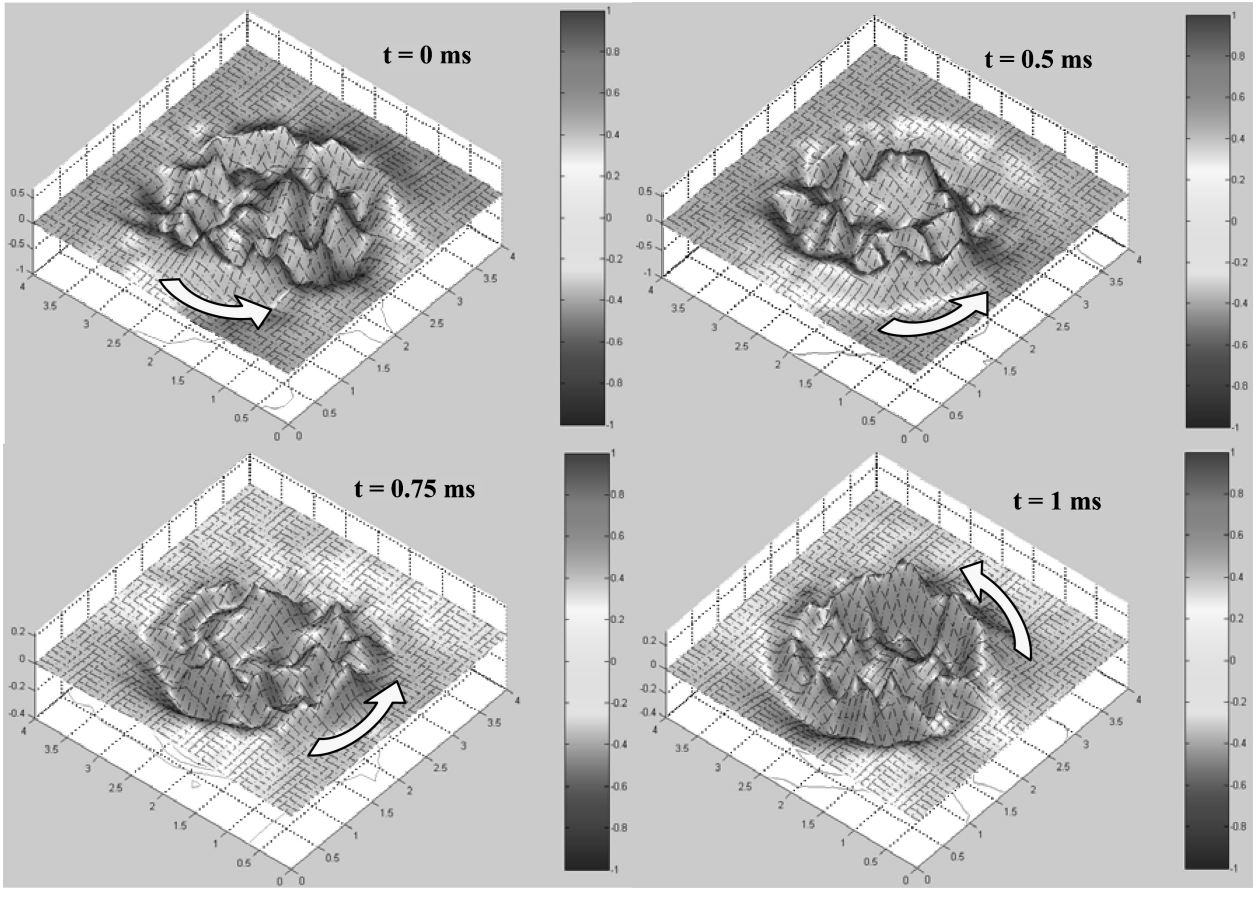


**Fig. 9 LSE estimates of the jet at four successive times.**

shown in Fig. 8. This result demonstrates the ability to estimate the fluctuating velocity by the mere use of the time signals of the near-field pressure as provided by the three microphones. It also shows that the LSE maintains the physical features of the flow because its dynamics can be extracted from the stochastic estimation of the velocity.

The hot-wire demonstration setup was quite simple and involved only a single wire probe and three microphones. This can be compared to previous experiments[21–23] in which rakes of x wires were used. Thus, significant information on the flow dynamics could be extracted from a minimal probes arrangement. However, because of the three-dimensional characteristic of this swirling flow and to obtain a better understanding of the flow dynamics, a PIV system that provided better spatial resolution of the flow coupled with more microphones was used to implement the LSE analysis.

### C. PIV Measurements

Two sets of data were acquired: velocities were measured in the stramwise plane and in the cross section of the jet.

#### 1. *Velocity Mapping in the Center Axial Plane*

The three velocity components along the axis plane of the TAS jet are shown in Fig. 10. The TAS is located at the top center of each image, and the flow is from top to bottom. The mean two-dimensional vector field shows the two main streams emanating from the external swirler (dark downward arrows) and the internal and external recirculation zones. The clockwise curved arrows show the entrainment of the ambient air at approximately 19 mm from the exhaust. The central recirculation zone is already present upstream as showed by the counterclockwise curved arrows and results in a counterflow in white up to 89 mm from the exhaust.

The mean axial and mean radial velocity contours verify the preceding observations. On the axial plot, the different zones are highlighted, and the recirculation zone in the center is shown separated from the external main flow.

The tangential velocity contour plot emphasizes the strong swirling characteristic of the flow by showing the out-of-plane tangential components of the velocity. In fact, the tangential velocity reaches high values of 18 m/s compared to the maximum axial velocity, which was about 22 m/s. If the geometric swirl number is defined as the ratio of the bulk tangential velocity to the bulk axial velocity, this number is nearly 1 in the main flow and 0.5 in the recirculation zone.

#### 2. *Application of the Linear Stochastic Estimation to Center-Plane Data*

The linear stochastic estimation is used here to describe the dynamics of the flow by using the near-field acoustic signal.

For the application of LSE, the three velocity components are described as

$$\hat{u}(x,t) = \sum_{i=1}^{n} L_i(x) P_i(t)$$

$$\hat{v}(x,t) = \sum_{i=1}^{n} M_i(x) P_i(t)$$

$$\hat{w}(x,t) = \sum_{i=1}^{n} N_i(x) P_i(t)$$

where $\hat{u}(x,t)$, $\hat{v}(x,t)$, and $\hat{w}(x,t)$ are the axial, radial, and tangential estimated fluctuating velocities, respectively; $n$ is the number of reference signals $P_i(t)$; and $L_i(x)$, $M_i(x)$, and $N_i(x)$ the estimation coefficients computed by the following linear system of equations:

$$\langle \tilde{u}(x,t) P_l(t) \rangle = \sum_{i=1}^{n} L_i(x) \langle P_i(t) P_l(t) \rangle$$

$$\langle \tilde{v}(x,t) P_l(t) \rangle = \sum_{i=1}^{n} M_i(x) \langle P_i(t) P_l(t) \rangle$$

$$\langle \tilde{w}(x,t) P_l(t) \rangle = \sum_{i=1}^{n} N_i(x) \langle P_i(t) P_l(t) \rangle$$

$$\text{for} \quad l = 1, \ldots, n \qquad (54)$$

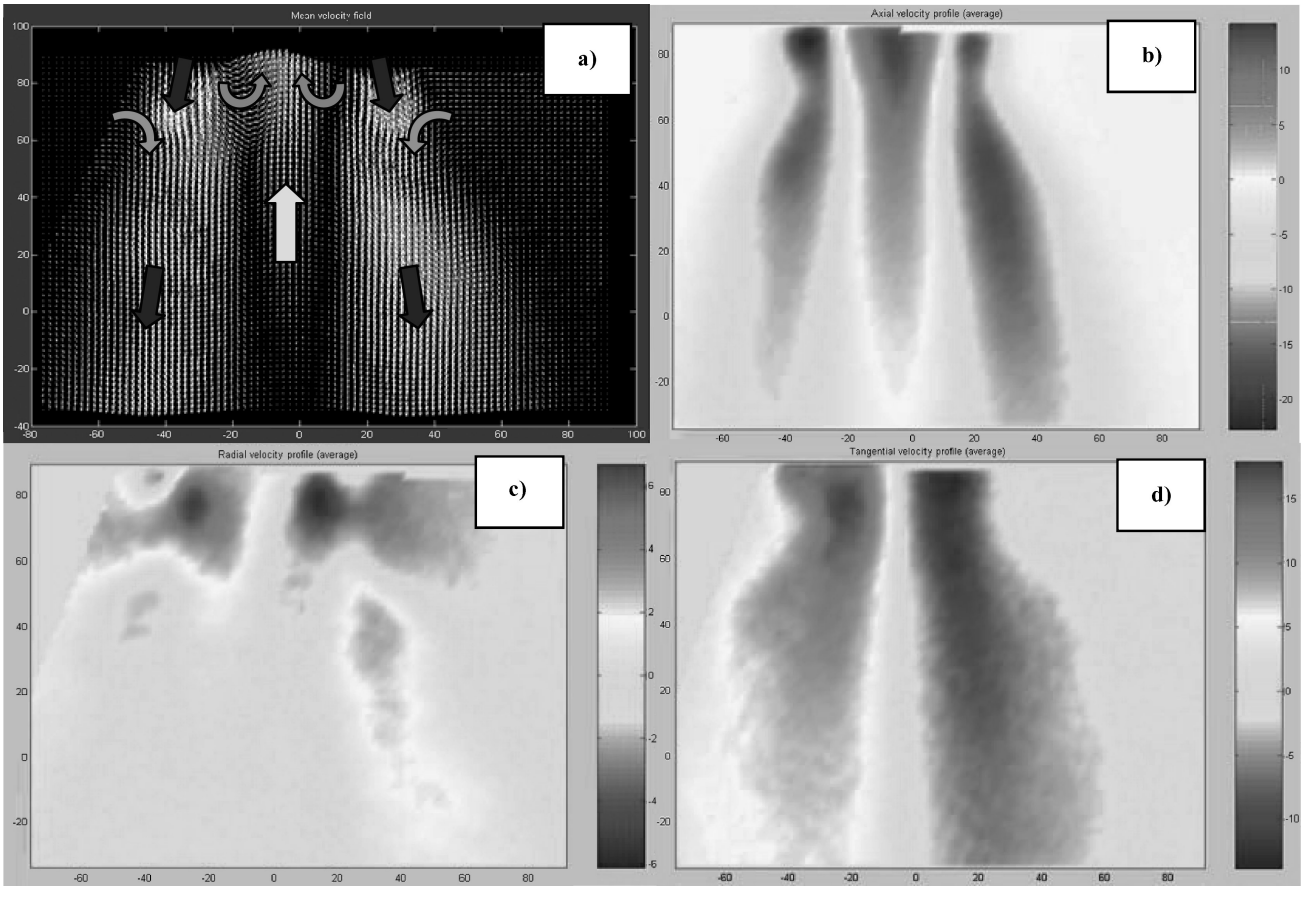


**Fig. 10 Mean velocity profiles of the TAS flow: a) mean vector field, b) mean axial velocity, c) mean radial velocity, and d) mean tangential velocity.**

where $\tilde{u}(x,t)$, $\tilde{v}(x,t)$, and $\tilde{w}(x,t)$ are the axial, radial, and tangential fluctuating velocities, respectively.

The coherent structures extracted by the linear estimate of the initial vector field are shown in Fig. 11b, where they are compared with the original data set (Fig. 11a). The LSE extracted from the flow three distinctive coherent structures that can be seen along the left-hand side of the jet. However, on the right-hand side of the plot, the coherence of the flow is not obvious. This asymmetry of the LSE profile is related to the features observed in the velocity/pressure correlations profiles of Fig. 7, where the correlations were only significant at the left-hand side of the jet. Thus, the microphones' input from the velocity field is restricted to the near field, and a complete and accurate estimate of the field would require microphones around the jet. The quality of the LSE analysis depends on the level and distribution of the correlations.

In spite of the low-level correlation, the LSE was able to extract the coherent structures from the turbulent background of the flow at the side of the jet adjacent to the microphones.

The LSE analysis resulted in approximately 99% reduction in data points' storage compared to the original data set. Once the estimation coefficients were computed, the LSE requires only data collected from reference probes (eight microphones in the present case), and there is no need for a complex and sometimes intrusive acquisition system. The other important advantage of the LSE is the ability to estimate a feature of the flow by using another parameter that can be not only different in nature but also remotely located; in the present case half of the velocity field was estimated by using the near-field acoustic signals of eight microphones. This feature can be very useful when it is necessary to collect data of a parameter that is not easily accessible or one that requires intrusive methods that would perturb the flow.

### *3. Velocity Mapping in the Cross-Sectional Plane*

Velocity measurements were performed in the cross section of the jet and are displayed in Figs. 12 and 13. Figure 12 shows the vector plot of the in-plane components of the mean velocity, that is, the

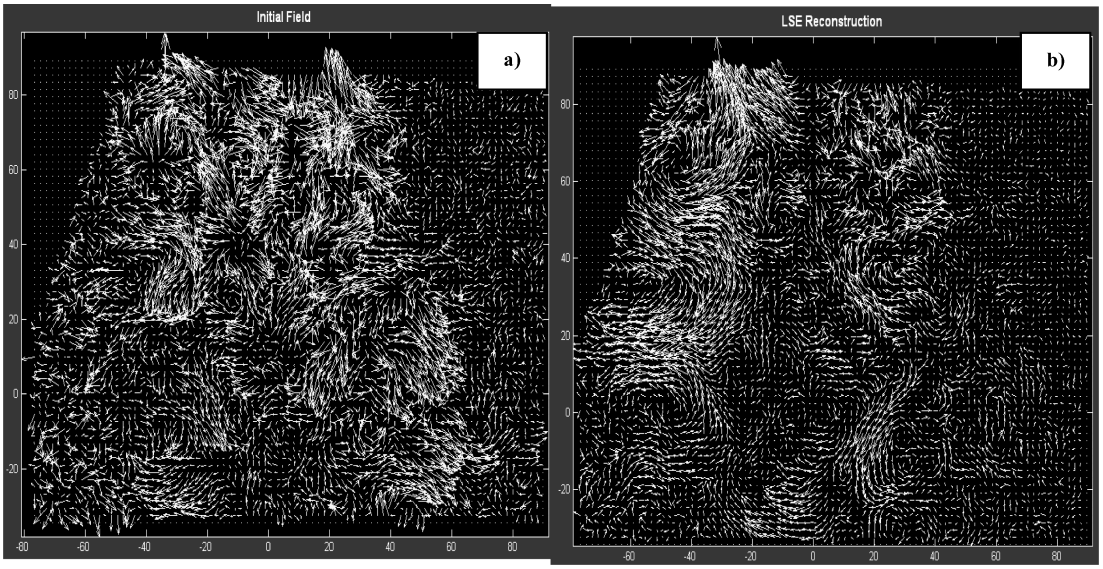


**Fig. 11 LSE reconstructions of an instantaneous flowfield: a) initial flowfield and b) LSE estimate.**

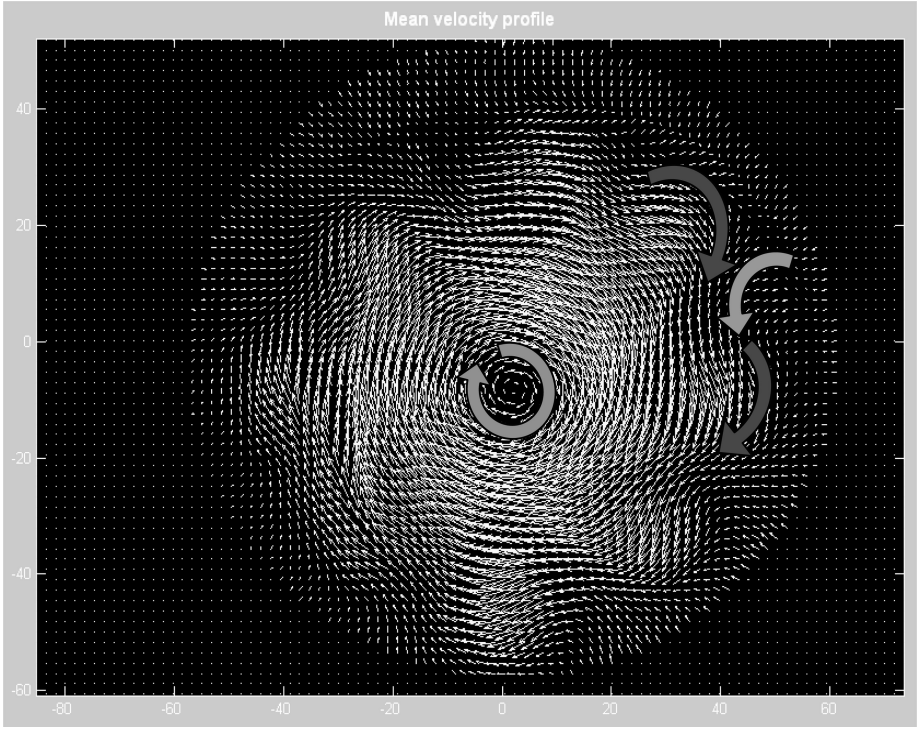


**Fig. 12 Mean cross-sectional vector field of the jet.**

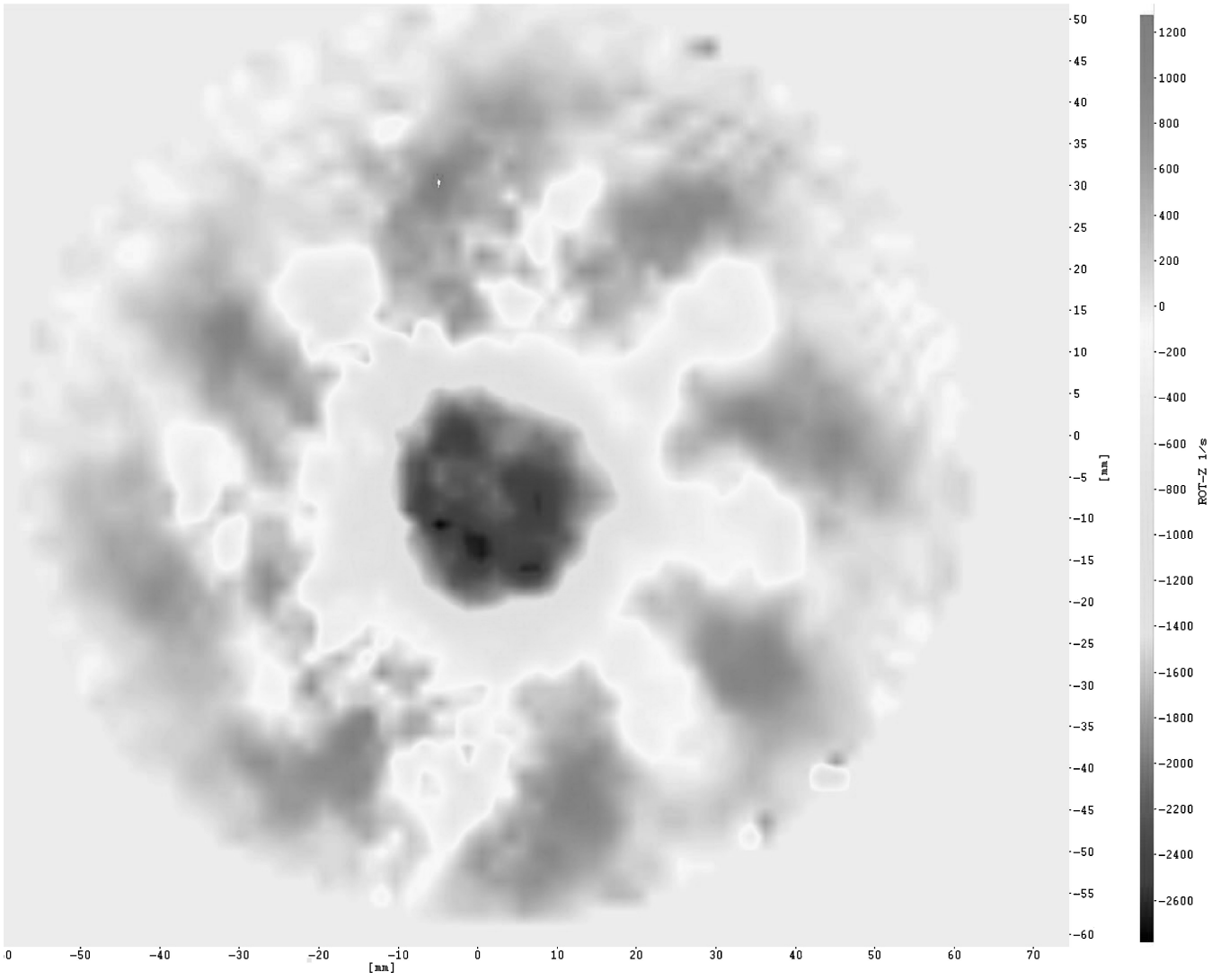


**Fig. 13 Axial vorticity of the jet.**

radial and tangential components. Eight lobes that are related to the outer swirler of the TAS can be identified around the jet edge. The core of the jet marked by the clockwise curved arrow is well defined and represents a strong rotational motion, which is the source of the large swirling structure. By entraining ambient air (light gray arrow) into the large vortical structure, the external lobes also contribute to the swirling motion of the jet. Figure 13 is a contour plot of the axial vorticity defined by $\omega = \partial u/\partial y - \partial v/\partial x$. The different zones identified earlier are clearly separated by the different shades of gray: the inner swirl in dark gray with a very high rotational shear, the external lobes in a light gray, and the zones of "entrainment" that are interlaced with the external lobes.

*4. Application of the Linear Stochastic Estimation to Cross-Sectional Data*

The reference signals that were used for the LSE computation were the eight microphones located circumferentially around the jet cross section. Because the quality of the estimation relies on the correlations between the reference signals and the velocity field and these correlations depend on the location of the reference probes, it is important to choose an optimal setup that maximizes the correlations.

In the present case, the correlations are higher in the proximity of the microphones (approximately 8 mm) and quickly decrease as the distance increases. Because the zones of high correlations are mostly confined to the microphones' neighborhood, these correlation profiles and thus the experimental setup are less favorable to a good estimation than in the previous experiments where the correlations were more distributed. Consequently, the LSE reconstruction of the flow is not as efficient as before. However, even for this less well-defined case it was possible to estimate quite well some of the 300 snapshots; an example of such estimation is depicted in Fig. 14, where an initial field issued from the PIV has been reconstructed with the LSE.

The LSE estimate was very efficient especially in the outer edge of the jet where the correlations were highest; the coherent motions slightly discernable in the initial flow field are also extracted and highlighted by the LSE. However the LSE is not as effective in the center of the jet.

The correlation levels obtained with the PIV snapshots are similar to those obtained using the hot wire (Figs. 7 and 8) so that both methods, though very different, yield similar results. The TAS flow is very turbulent in its cross section and consequently has a significant incoherent component that cannot be extracted by the linear stochastic estimation. The very high shear level that exists in the cross-sectional flow hampers the ability of the microphones to detect features of the innermost flow, and thus their capability of being affected by the flowfield is restricted to the edge of the jet, yielding an unbalanced reconstruction between the outer and the inner sections of the flow.

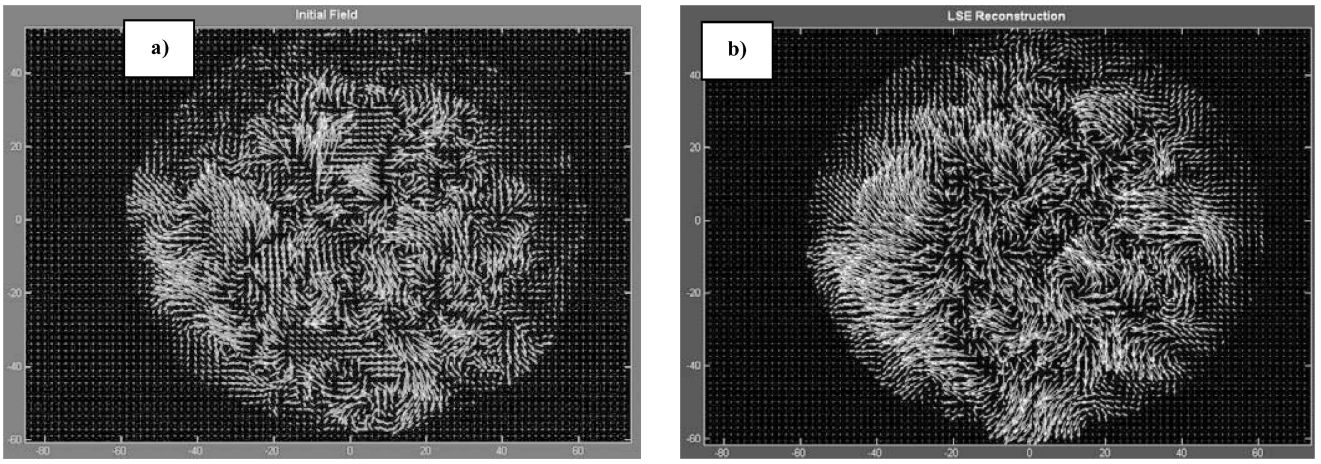


**Fig. 14 LSE reconstruction in a cross-sectional plane: a) initial flowfield and b) LSE estimate.**

## IV. Summary

LSE analysis was performed in a highly swirling and turbulent flow produced by a triple annular swirler. The estimation provided by the LSE was not equally effective in all of the regions of the jet because of the high turbulence and low levels of correlation throughout the jet. It is expected that in flow with lower turbulence intensity the technique will be even more accurate.

In general, LSE was shown to be an efficient method for the extraction of coherent structures from a turbulent flowfield and to capture their dynamic behavior even in the present flowfield with local turbulence intensity greater than 100%. Indeed such a filtering technique brings a real advantage in data reduction because it allows the representation of the most energetic characteristics of the flow with a minimum amount of data resulting in a data-reduction ratio of approximately 99%.

It was demonstrated that the LSE highly depends on the level of correlation and consequently requires special care in setting the synchronization of the acquisition methodology. Another consequence of this dependence is that the LSE is not as accurate for highly turbulent flows such as the present swirling flow because the high incoherence of the flow results in a low level of correlation necessary for a good estimation. However, even in the present flow with large region of recirculation, reverse flow, and extremely high turbulence level, it was possible to capture the dominant features of the flow with only the microphones. The present work is limited to nonreacting and relatively low velocity flow. The present technique was also shown to be effective in high subsonic jets. It remains to be shown that it can also be applied to reacting flows and other flows with large density gradients.

The LSE can be considered as an alternative to classical data acquisition. The advantage of the concept of LSE is in the fact that it allows collecting data of a certain parameter without having to directly measure it. It also enables data collection with no intrusion. The ability to recreate the flowfield and its coherent structures was demonstrated here solely from the temporal signals issued by eight microphones that were placed near the jet.

One of the main advantages of the LSE is that the resulting estimated flow can be used to generate realistic inlet BCs for large-eddy simulation or DNS instead of computing the complete transition that is typically required to initiate the computations of a turbulent flowfield. Such realistic inflow conditions can save significant computational time because the LSE only requires a minimum number of probes to describe the turbulent flow. Moreover, these numerical simulations often suffer from a lack of physical and realistic input, which includes not only mean quantities but also information on the flow dynamics and turbulent structures statistics. Consequently, the LSE turns out to be a practical tool to generate realistic turbulent inflow interfacing between unsteady CS experimental data and numerical simulations.

## Acknowledgments

This research was performed with support from the office of Naval Research, monitored by Stephen W. McElvany, Environmental Quality Program Officer.

## References

[1]Hussain, F., "Role of Coherent Structures in Turbulent Shear Flows," *Proceedings of the Indian Academy of Science and Engineering Science*, Vol. 4, No. 2, 1981, pp. 129–181.

[2]Hussain, F., "Coherent Structure—Reality and Myth," *Physics of Fluids*, Vol. 26, No. 10, 1983, pp. 2816–2850.

[3]Lesieur, M., *Turbulence in Fluids*, 2nd ed., Kluwer, Dordrecht, The Netherlands, 1990.

[4]Adrian, R. J., and Moin, P., "Stochastic Estimation of Organized Turbulent Structure: Homogeneous Shear Flow," *Journal of Fluid Mechanics*, Vol. 190, 1988, pp. 531–559.

[5]Papoulis, A., *Probability, Random Variables, and Stochastic Processes*, McGraw–Hill, New York, 1965.

[6]Bonnet, J. P., "Eddy Structure Identification," *CISM Courses and Lectures*, No. 353, Springer-Verlag, Vienna, 1996.

[7]Bonnet, J. P., Cole, D. R., Delville, J., Glauser, M. N., and Ukeiley, L. S., "Stochastic Estimation and Proper Orthogonal Decomposition: Complementary Techniques for Identifying Structure," *Experiments in Fluids*, Vol. 17, No. 5, 1994, pp. 307–314.

[8]Druault, P., "Developments of Experimental/Computational Interfaces. Application to a Turbulent Mixing Layer," Ph.D. Dissertation, Univ. of Poitiers, Poitiers, France, 1996.

[9]Bonnet, J. P., Delville, J., Glauser, M. N., Antonia, R. A., Bisset, D. K., Cole, D. R., Fiedler, H. E., Garem, J. H., Hilberg, D., Jeong, J., Kevlahan, N. K. R., Ukeiley, L. S., and Vincendeau, E., "Collaborative Testing of Eddy Structure Identification Methods in Free Turbulent Shear Flows," *Experiments in Fluids*, Vol. 25, No. 3, 1998, pp. 197–225.

[10]Lewalle, J., Delville, J., and Bonnet, J. P., "Decomposition of Mixing Layer Turbulences into Coherent Structures and Background Fluctuations," *Flow Turbulence and Combustion*, Vol. 64, No. 4, 2000, pp. 301–328.

[11]Picard, C., and Delville, J., "Pressure Velocity Coupling in a Subsonic Round Jet," *International Journal of Heat and Fluid Flow*, Vol. 21, No. 3, 2000, pp. 359–364.

[12]George, W. K., and Davidson, L., "Role of Initial Conditions in Establishing Asymptotic Flow Behavior," *AIAA Journal*, Vol. 42, No. 3, 2004, pp. 438–446.

[13]Druault, P., Lardeau, S., Bonnet, J. P., Coiffet, F., Delville, J., Lamballais, E., Largeau, J. F., and Perret, L., "Generation of Three-Dimensional Turbulent Inlet Conditions for Large-Eddy Simulation," *AIAA Journal*, Vol. 42, No. 3, 2004, pp. 447–456.

[14]Grinstein, F. F., "Open Boundary Conditions in the Simulation of Subsonic Turbulent Shear Flows," *Journal of Computational Physics*, Vol. 115, No. 1, 1994, pp. 43–55.

[15]Sagaut, P., *Large Eddy Simulation for Incompressible Flows*, Springer-Verlag, New York, 2002.

[16]Lund, T. S., Wu, X., and Squires, K. D., "On the Generation of Turbulent Inflow Conditions for Boundary-Layer Simulations," AIAA Paper 2003-0067, 2003; also *Journal of Computational Physics*, Vol. 140, No. 2, 1998, pp. 233–258.

[17]Keating, A., and Kaltenbach, H. J., "A Priori and A Posteriori Tests of Inflow Conditions for Large-Eddy Simulation," *Physics of Fluids*, Vol. 16, No. 12, 2004, pp. 4696–4712.

[18]Grinstein, F. F., Young, T. R., Gutmark, E. J., Li, G., Hsiao, G., and Mongia, H. C., "Flow Dynamics in a Swirl Combustor," *Journal of Turbulence*, Vol. 3, No. 1, 2002, p. 1468.

[19]Schlüter, J. U., Pitsch, H., and Moin, P., "Outflow Conditions for Integrated Large Eddy Simulation/Reynolds-Averaged Navier–Stokes Simulations," *AIAA Journal*, Vol. 42, No. 3, 2004, pp. 478–484.

[20]Li, G., and Gutmark, E. J., "LDV and PIV Study of Velocity Flow Field for a Multiple Swirl Spray Combustor," AIAA Paper 2002-4010, July 2002.

[21]Bonnet, J. P., Coiffet, F., and Delville, J., "The Generation of Realistic 3D Unsteady Inlet Conditions for LES," AIAA Paper 2003-0065, Jan. 2003.

[22]Bonnet, J. P., and Delville, J., "Review of Coherent Structures in Turbulent Free Shear Flows and Their Possible Influence on Computational Methods," *Flow, Turbulence and Combustion*, Vol. 66, No. 4, 2001, pp. 333–353.

[23]Bonnet, J. P., and Glauser, M. N. (eds.), *Eddy Structure Identification in Free Turbulent Shear Flows*, Kluwer Academic, Dordrecht, The Netherlands, 1993.

C. Kaplan
*Associate Editor*